



4-Oxobenzo[d]1,2,3-triazin-pyridinium-phenylacetamide derivatives as new anti-Alzheimer agents: design, synthesis, in vitro evaluation, molecular modeling, and molecular dynamic study

Fahimeh Hosseini¹ · Maryam Mohammadi-Khanaposhtani² · Homa Azizian³ · Ali Ramazani¹ · Maliheh Barazandeh Tehrani⁴ · Hamid Nadri⁵ · Bagher Larijani⁶ · Mahmoud Biglar⁶ · Hossein Adibi⁶ · Mohammad Mahdavi⁶

Received: 6 October 2019 / Accepted: 3 December 2019
© Springer Science+Business Media, LLC, part of Springer Nature 2020

Abstract

A new series of 4-oxobenzo[d]1,2,3-triazin-pyridinium-phenylacetamide hybrids **8a–p** was designed, synthesized, and screened as the potential cholinesterase inhibitors against acetylcholinesterase (AChE) and butyrylcholinesterase (BuChE). Obtained anti-cholinesterase activities demonstrated that all the title compounds exhibited excellent inhibition against BuChE and moderate inhibitory activity toward AChE in comparison to standard cholinesterase inhibitor donepezil. For example, compound **8e** exhibited about 49-fold higher inhibitory activity than donepezil ($IC_{50} = 3.2 \pm 0.3 \mu M$) against BuChE. This compound inhibited BuChE via a mixed-type inhibition mode. This finding demonstrated that compound **8e** in addition to catalytic anionic site (CAS) can also interact with the peripheral anionic site (PAS) of BuChE. Molecular modeling and molecular dynamic studies were also performed on synthesized compounds.

Keywords Anti-Alzheimer · 4-Oxobenzo[d]1,2,3-triazin · Phenylacetamide · Molecular dynamic · Molecular modeling

Introduction

Alzheimer's disease (AD) is a neurodegenerative disorder with main clinical manifestations such as progressive memory loss, language deterioration, and severe cognitive decline [1]. The most common cause of dementia in the elderly people is

AD [2]. The exact pathogenic mechanism of this disease remains unclear but researchers suggests that factors such as decrease neurotransmitter acetylcholine (ACh) level in the hippocampal and cortical regions of the brain, the abnormal deposition of β -amyloid peptides ($A\beta$), the formation of neurofibrillary tangles, oxidative stress, and

Fahimeh Hosseini and Maryam Mohammadi-Khanaposhtani contributed equally to this work.

Electronic supplementary material The online version of this article (<https://doi.org/10.1007/s11224-019-01472-0>) contains supplementary material, which is available to authorized users.

✉ Ali Ramazani
aliramazani@znu.ac.ir

✉ Mohammad Mahdavi
momahdavi@tums.ac.ir

¹ Department of Chemistry, University of Zanjan, P.O. Box 45195-313, Zanjan, Iran

² Cellular and Molecular Biology Research Center, Health Research Institute, Babol University of Medical Sciences, Babol, Iran

³ Department of Medicinal Chemistry, School of Pharmacy-International Campus, Iran University of Medical Sciences, Tehran, Iran

⁴ Department of Medicinal Chemistry, Faculty of Pharmacy, Tehran University of Medical Sciences, Tehran, Iran

⁵ Department of Medicinal Chemistry, Faculty of Pharmacy and Pharmaceutical Sciences Research Center, Shahid Sadoughi University of Medical Sciences, Yazd, Iran

⁶ Endocrinology and Metabolism Research Center, Endocrinology and Metabolism Clinical Sciences Institute, Tehran University of Medical Sciences, Tehran, Iran

biometallic dysregulation can be involved in the creation and progression of AD [3].

Today, the most common treatment for AD is the use of acetylcholinesterase (AChE) inhibitors in order to increase the synaptic levels of ACh, because AChE is responsible for the degradation of ACh in the brain [4]. Another enzyme that can partially degrade ACh in the brain is butyrylcholinesterase (BuChE) [5]. Recently, several evaluations revealed that with the progress of AD, AChE activity in the brain of patients is gradually decreased while BuChE activity is significantly increased [6]. Therefore, inhibition of both of these enzymes may be useful in the treatment of AD [7, 8].

During the last decade, our research group using the molecular hybridization approach has introduced numerous structures with anti-Alzheimer's activities [9, 10]. Recently, we reported 4-oxobenzo[d]1,2,3-triazin-benzyl pyridinium derivatives **A** as novel potent AChE inhibitors [11]. On the other hand, phenylacetamide derivatives **B** showed the inhibitory activity against AChE [12]. Therefore, herein, in order to design new cholinesterase (ChE) inhibitors, we replaced benzyl group of the scaffold **A** with phenylacetamide moiety of scaffold **B**; designed 4-oxobenzo[d]1,2,3-triazin-pyridinium-phenylacetamide hybrids **8a–p** were synthesized and evaluated for their in vitro ChE inhibitory activities against AChE and BuChE. Furthermore, molecular modeling and molecular dynamic studies were performed to evaluation interactions of the synthesized compounds with AChE and BuChE.

Experimental details

Material and methods

Melting points of 4-oxobenzo[d]1,2,3-triazin-pyridinium-phenylacetamide hybrids **8a–p** were measured on a Kofler hot stage apparatus. The NMR (^1H and ^{13}C) and IR spectra of the title compounds were obtained by using a Bruker FT-500 and Nicolet Magna FTIR 550 spectrophotometer (KBr disks), respectively. Elemental analysis was measured by an Elementar Analysensystem GmbH VarioEL CHNS mode.

Cholinesterase inhibition assay

The target enzymes (AChE (E.C. 3.1.1.7, type V-S, lyophilized powder, from electric eel, ≥ 1000 units/mg protein) and BuChE (E.C. 3.1.1.8, from equine serum)), substrates (acetylthiocholine iodide and butyrylthiocholine iodide), indicator (DTNB [5,5'-dithiobis(2-nitrobenzoic acid)]), and standard drug (donepezil) were purchased from Sigma-Aldrich. The anti-cholinesterase activity of 4-

oxobenzo[d]1,2,3-triazin-pyridinium-phenylacetamide hybrids **8a–p** was assessed by Ellman's method [13]. DMSO (1 mL) was used as the solvent for dissolving the title compounds and preparing appropriate stock. The stock of the synthesized compounds was diluted by using phosphate buffer to achieve final concentrations. A mixture of phosphate buffer (0.1 M, pH = 8.0, 50 μL), DTNB (0.1 M, 125 μL), AChE or BuChE (0.2 U/ml, 25 μL), and yeast compound (25 μL) was incubated for 5 min at room temperature. Then, acetylthiocholine iodide or butyrylthiocholine iodide (0.01 M, 10 μL) was added, and the change of the absorbance was measured at 405 nm after 15 min. Synergy HTX Multi-Mode Reader (BioTek) was used for these assays.

Kinetic study of BuChE inhibition

The inhibition mode and K_i value of the most BuChE inhibitor **8e** were determined by the modified Ellman's method. The related experiments in this step were performed similar to the enzyme inhibition assay. The rate of enzymatic reaction was measured in the different concentrations of the compound **8e** (0, 30, 60, and 120 nM) in order to draw Lineweaver–Burk reciprocal plots to estimate the type of inhibition. Finally, slopes of the latter plots were plotted against the different concentrations of the test compound **8e** in order to determine K_i value. Enzymatic reactions were performed in triplicate, and data analysis was performed by Microsoft Excel 2013.

Target and ligand preparation

In order to find out the interaction modes of the synthesized compounds over ChEs, Maestro Molecular Modeling platform (version 11.5: Schrodinger, LLC: New York, NY, 2018) was performed [14]. Initially, the proper crystal structures of AChE (PDB code: 6o4w) and BuChE (PDB code: 4bds) were retrieved from the Protein Data Bank (<http://www.rcsb.org>) [15, 16]. These pdb ids were selected based on criteria like highest resolution (\AA), being related to *Homo sapiens* species, wild type with no modified residue, and the existence of co-crystallized ligand. As the prosthetic group and the co-factors are not directly involved in ChE inhibition, so they totally removed before docking investigation. Except the four structural waters molecule in the AChE and BuChE active site, which bridge the receptor important residues by way of hydrogen bond and conserve among other species, the rest of the water molecules were removed from crystallographic structures of the target enzymes [17]. The 2D structures of all synthesized compounds were drawn in Marvin 15.10.12.0 program and converted into pdb (<http://www.chemaxon.com>). The Protein Preparation

Wizard and the LigPrep module were used to prepare protein and ligand structure properly [18].

Docking protocol

The appropriate pose for the compounds over AChE and BuChE was determined by induced fit docking protocol (IFD) [18]. At the active site of AChE and BuChE, the co-crystallized ligand (donepezil and tacrine, respectively) was used to generate the grid for IFD calculation. The maximum 20 poses with receptor and ligand Van der Waals radii of 0.7 and 0.5, respectively, were considered. Residues within 5 Å of the donepezil and tacrine at the active site were refined followed by side-chain optimization. Structures whose prime energy is more than 30 Kcal/mol eliminated based on extra precious glide docking. The energetically favorable IFD complexes were obtained for compounds and applied to MD simulation.

Molecular dynamics simulation

Molecular simulations of this study were performed using the Desmond v5.3 using Maestro interface (from Schrödinger 2018–4 suite) [18]. We evaluated the stability of the best drug candidate from the experimental study, compound **8p** and **8e** over AChE and BuChE, respectively, and compared their perturbation with the standard inhibitor donepezil.

In order to building system for MD simulation, the protein-ligand complexes were solvated by SPC explicit water molecules and placed in the center of an orthorhombic box of appropriate size in the Periodic Boundary Condition (PBC). Sufficient counter-ions and a 0.15 M solution of NaCl also utilized to neutralize the system and to simulate the real cellular ionic concentrations, respectively. The MD protocol involved minimization, pre-production, and finally production of MD simulation steps. In the minimization procedure, the entire system was allowed to relax for 2500 steps by the steepest descent approach. Then, the temperature of the system was raised from 0 to 300 K by applying a small force constant on the enzyme in order to restrict any drastic changes. MD simulations were performed via NPT (constant number of atoms, constant pressure, i.e., 1.01325 bar and constant temperature, i.e., 300 K) ensemble. The Nose-Hoover chain method was used as the default thermostat with 1.0 ps interval and Martyna-Tobias-Klein as the default barostat with 2.0-ps interval by applying isotropic coupling style. Long-range electrostatic forces were calculated based on particle-mesh-based Ewald approach with the cut-off radius for coulombic forces set to 9.0 Å. Finally, this system subjected to production MD simulations for 20 ns for each protein-ligand complex. During the simulation, every 1000 ps of the actual frame was stored. The dynamic behavior and structural changes of the systems were analyzed by the calculation of energy and the root mean square deviation (RMSD). Subsequently, by using

trajectory-clustering tool, the representative structure with the largest number of neighbors from the equilibrated trajectory was evaluated for investigation of each ligand-protein complex.

Prime MM-GBSA

The ligand binding energies (ΔG_{bind}) were calculated using Molecular Mechanics/Generalized Born Surface Area (MM-GBSA) modules (Schrödinger LLC 2018) [18] based on the following equation: $\Delta G_{\text{Bind}} = E_{\text{Complex}} - [E_{\text{Receptor}} + E_{\text{Ligand}}]$, where ΔG_{Bind} is the calculated relative free energy which includes both ligand and receptor strain energy. E_{Complex} is the MM-GBSA energy of the minimized complex, and E_{Ligand} is the MM-GBSA energy of the ligand after removing it from the complex and allowing it to relax. E_{Receptor} is the MM-GBSA energy of relaxed protein after separating it from the ligand. The MM-GBSA calculation performed on the structures with the higher number of neighbors in cluster was obtained from MD simulation trajectory.

General procedure for the synthesis of pyridine derivatives **3a–b**

A mixture of isatoic anhydride **1** (1 mmol) and pyridin-3-ylmethanamine **2a** or pyridin-4-ylmethanamine **2b** (1 mmol) in water (15 mL) was stirred at room temperature for 8 h. Then, the reaction mixture was filtered off and the precipitates were collected and washed with water to obtain pure pyridine derivatives **3a–b**.

General procedure for the produce of **3** or **4**-(pyridin) benzo[d][1,2,3]triazin-4(3H)-ones **4a–b**

A suspension of the pyridine derivatives **3a–b** (1 mmol), sodium nitrite (1 mmol), and hydrochloride acid 37% (1 mL) in water (5 mL) was stirred at 0 °C for 10 min. Then, the obtained residue was cooled to 4 °C and filtered off and the participates were washed with the mixture of water/ethanol to give pure **3** or 4-(pyridin)benzo[d][1,2,3] triazin-4(3H)-ones **4a–b**.

General procedure for the synthesis of *N*-phenyl-2-chloroacetamides **7a–h**

A mixture of aniline derivatives **5a–h** and chloroacetyl chloride **6** in DMF was stirred at room temperature for 30 min. Then, the reaction mixture was diluted with water, poured into crashed ice, and the obtained precipitate were filtered off. Finally, residue was washed with cold water to obtain pure *N*-phenyl-2-chloroacetamides **7a–h**.

General procedure for the synthesis of 4-oxobenzo[d][1,2,3-triazin-pyridinium-phenylacetamides 8a–p

The *N*-phenyl-2-chloroacetamides **7a–h** (1 mmol) were added to the stirred solution of compounds **4a–b** (1 mmol) in dry acetonitrile (10 mL), and the final mixture was heated at reflux for 2–3 h. Upon completion (checked by TLC), acetonitrile was evaporated and *n*-hexane (20 mL) was added to the residue and obtained precipitates were separated by filtration and washed with *n*-hexane to afford the pure title compounds **8a–p**.

1-(2-Oxo-2-(phenylamino)ethyl)-3-((4-oxobenzo[d][1,2,3]triazin-3(4H)-yl)methyl)pyridin-1-ium chloride (8a)

Yellow solid; yield: 68%; mp: 198–200 °C. IR (KBr): $\nu = 3232, 3080, 3042, 2840, 1694, 1682, 1640, 1600, 1546, 1465, 1337, 1299, 1250, 1199, 1075, 952, 904$. ^1H NMR (CDCl_3 , 250 MHz): $\delta = 10.60$ (s, 1H, NH), 9.07–9.02 (m, 2H), 8.75 (s, 1H), 8.21–7.93 (m, 5H), 7.49 (m, 2H), 7.28 (m, 2H), 7.03 (s, 1H), 5.80 (s, 2H, CH_2), 5.61 (s, 2H, CH_2). ^{13}C NMR (CDCl_3 , 62.9 MHz): $\delta = 163.1, 155.5, 146.0$ (2C), 145.5, 143.9, 138.2, 136.5, 136.2, 133.8, 129.3 (2C), 128.6, 127.7, 125.0, 124.4, 119.5 (2C), 62.4, 50.0. Anal. calcd for $\text{C}_{21}\text{H}_{18}\text{ClN}_5\text{O}_2$ (407.85): C, 61.84; H, 4.45; N, 17.17; found: C, 62.87; H, 4.49; N, 17.18.

1-(2-Oxo-2-(*p*-tolylamino)ethyl)-3-((4-oxobenzo[d][1,2,3]triazin-3(4H)-yl)methyl)pyridin-1-ium chloride (8b)

Cream solid; yield: 70%; mp: 123–125 °C. IR (KBr): $\nu = 3420, 3030, 2923, 1685, 1616, 1577, 1512, 1478, 1428, 1332, 1293, 1058, 912$. ^1H NMR (CDCl_3 , 250 MHz): $\delta = 10.75$ (s, 1H, NH), 9.12 (s, 1H), 9.01 (d, $J = 5$ Hz, 2H), 8.78 (d, $J = 7.5$ Hz, 1H), 8.17–8.77 (m, 5H), 7.44 (d, $J = 5.5$ Hz, 2H), 7.08 (d, $J = 5.5$ Hz, 2H), 5.83 (s, 2H, CH_2), 5.59 (s, 2H, CH_2), 2.20 (s, 3H, CH_3). ^{13}C NMR (CDCl_3 , 62.9 MHz): $\delta = 164.8, 155.2, 146.1, 145.2, 144.1, 136.2, 135.9, 133.5, 133.2, 132.4, 129.6$ (2C), 128.5, 125.0, 124.1, 120.3, 119.5 (2C), 62.3, 50.6, 20.8. Anal. calcd for $\text{C}_{22}\text{H}_{20}\text{ClN}_5\text{O}_2$ (421.88): C, 62.63; H, 4.78; N, 16.60; found: C, 62.53; H, 4.75; N, 16.67.

1-(2-((4-Methoxyphenyl)amino)-2-oxoethyl)-3-((4-oxobenzo[d][1,2,3]triazin-3(4H)-yl)methyl)pyridin-1-ium chloride (8c)

Yellow solid; yield: 75%; mp: 144–146 °C. IR (KBr): $\nu = 3425, 3031, 2851, 1685, 1604, 1577, 1510, 1470, 1428, 1294, 1059, 912$. ^1H NMR (CDCl_3 , 250 MHz): $\delta = 10.42$ (s,

1H, NH), 9.13 (s, 1H), 9.04 (d, $J = 5$ Hz, 1H), 8.78 (d, $J = 7.5$ Hz, 1H), 8.19–7.89 (m, 5H), 7.51 (d, $J = 7.75$ Hz, 2H), 6.86 (d, $J = 7.75$ Hz, 2H), 5.83 (s, 2H, CH_2), 5.65 (s, 2H, CH_2). ^{13}C NMR (CDCl_3 , 62.9 MHz): $\delta = 162.8, 155.9, 155.2, 146.2, 145.5, 144.1, 136.4, 135.9, 133.5, 132.4, 128.5, 127.6, 125.0, 124.2, 121.0$ (2C), 119.8, 114.4 (2C), 62.5, 55.5, 50.6. Anal. calcd for $\text{C}_{22}\text{H}_{20}\text{ClN}_5\text{O}_3$ (437.88): C, 60.34; H, 4.60; N, 15.99; found: C, 60.38; H, 4.51; N, 15.78.

1-(2-((3,4-Dimethoxyphenyl)amino)-2-oxoethyl)-3-((4-oxobenzo[d][1,2,3]triazin-3(4H)-yl)methyl)pyridin-1-ium chloride (8d)

Cream solid; yield: 70%; mp: 175–177 °C. IR (KBr): $\nu = 3225, 3172, 3044, 2925, 2849, 1698, 1642, 1596, 1541, 1491, 1401, 1248, 1090, 918, 829$. ^1H NMR (CDCl_3 , 250 MHz): $\delta = 10.45$ (s, 1H, NH), 9.05–9.01 (m, 2H), 8.78 (d, $J = 5$ Hz, 1H), 8.20–7.94 (m, 6H), 7.22–7.23 (m, 1H), 7.02–6.86 (m, 2H), 5.78 (s, 2H, CH_2), 5.58 (s, 2H, CH_2). ^{13}C NMR (CDCl_3 , 62.9 MHz): $\delta = 162.0, 155.7, 155.5, 148.7, 146.0, 145.4, 144.0, 136.7, 136.2, 133.8, 131.9, 128.7, 125.0, 119.9, 112.5, 104.5, 62.4, 56.3, 55.9, 50.0$. Anal. calcd for $\text{C}_{23}\text{H}_{22}\text{ClN}_5\text{O}_4$ (467.9): C, 59.04; H, 4.74; N, 14.97; found: C, 59.05; H, 4.65; N, 14.73.

1-(2-((4-Chlorophenyl)amino)-2-oxoethyl)-3-((4-oxobenzo[d][1,2,3]triazin-3(4H)-yl)methyl)pyridin-1-ium chloride (8e)

Cream solid; yield: 80%; mp: 175–177 °C. IR (KBr): $\nu = 3253, 3187, 3042, 2852, 1697, 1681, 1648, 1601, 1541, 1491, 1401, 1290, 1247, 1081, 985, 827$. ^1H NMR (CDCl_3 , 250 MHz): $\delta = 10.67$ (s, 1H, NH), 9.07–9.04 (m, 2H), 8.73 (s, 1H), 8.14–7.93 (m, 5H), 7.49 (d, $J = 5$ Hz, 2H), 7.30 (d, $J = 5$ Hz, 2H), 5.75 (s, 2H, CH_2), 5.63 (s, 2H, CH_2). ^{13}C NMR (CDCl_3 , 62.9 MHz): $\delta = 163.4, 156.4, 149.7, 144.0, 141.2, 137.2, 136.5, 136.2, 133.8, 129.7, 129.1$ (2C), 128.6, 127.8, 125.0, 121.3 (2C), 120.9, 119.8, 62.6, 50.0. Anal. calcd for $\text{C}_{21}\text{H}_{17}\text{Cl}_2\text{N}_5\text{O}_2$ (442.3): C, 57.03; H, 3.87; N, 15.83; found: C, 57.07; H, 3.85; N, 15.78.

1-(2-((2,3-Dichlorophenyl)amino)-2-oxoethyl)-3-((4-oxobenzo[d][1,2,3]triazin-3(4H)-yl)methyl)pyridin-1-ium chloride (8f)

Cream solid; yield: 68%; mp: 146–148 °C. IR (KBr): $\nu = 3455, 3030, 2923, 1686, 1605, 1578, 1478, 1429, 1332, 1293, 1050, 912$. ^1H NMR (CDCl_3 , 250 MHz): $\delta = 10.53$ (s, 1H, NH), 9.12 (s, 1H), 9.01 (d, $J = 4.6$ Hz, 1H), 8.76 (d, $J = 7.5$ Hz, 1H), 8.24–8.07 (m, 5H), 7.92 (t, $J = 7.5$ Hz, 1H), 7.69 (t, $J = 8$ Hz, 1H), 7.48 (d, $J = 7.5$ Hz, 1H), 7.37 (d, $J = 7.5$ Hz, 1H), 5.82 (s, 2H, CH_2), 5.69 (s, 2H, CH_2). ^{13}C NMR (CDCl_3 , 62.9 MHz): $\delta = 163.6, 155.2, 146.3,$

145.1, 144.1, 138.7, 136.3, 136.0, 133.5, 133.2, 132.4, 128.6, 127.6, 129.6, 128.5 (2C), 125.0, 124.2, 119.8, 62.2, 50.6. Anal. calcd for $C_{21}H_{16}Cl_3N_5O_2$ (476.74): C, 52.91; H, 3.38; N, 14.69; O, 6.71; found: C, 52.23; H, 3.41; N, 16.79.

1-(2-((4-Bromophenyl)amino)-2-oxoethyl)-3-((4-oxobenzod[1,2,3]triazin-3(4H)-yl)methyl)pyridin-1-ium chloride (8g)

Cream solid; yield: 76%; mp: 151–153 °C. IR (KBr): $\nu = 3425, 3030, 2851, 1686, 1606, 1589, 1549, 1478, 1428, 1293, 1026, 912$. 1H NMR ($CDCl_3$, 250 MHz): $\delta = 10.73$ (s, 1H, NH), 9.13 (s, 1H), 9.05 (d, $J = 4.7$ Hz, 1H), 8.78 (d, $J = 7.5$ Hz, 1H), 8.18–8.01 (m, 5H), 7.57 (d, $J = 7.25$ Hz, 2H), 7.46 (d, $J = 7.25$ Hz, 2H), 5.83 (s, 2H, CH_2), 5.69 (s, 2H, CH_2). ^{13}C NMR ($CDCl_3$, 62.9 MHz): $\delta = 163.7, 155.2, 146.2, 145.5, 144.1, 138.3, 138.1, 136.7, 135.9, 133.5, 132.6, 132.0, 128.5, 127.6, 125.0, 124.3, 121.6, 119.8, 62.7, 50.0$. Anal. calcd for $C_{21}H_{17}BrClN_5O_2$ (486.75): C, 51.82; H, 3.52; N, 14.39; found: C, 51.83; H, 3.56; N, 14.38.

1-(2-((4-Nitrophenyl)amino)-2-oxoethyl)-3-((4-oxobenzod[1,2,3]triazin-3(4H)-yl)methyl)pyridin-1-ium chloride (8h)

Cream solid; yield: 690%; mp: 158–160 °C. IR (KBr): $\nu = 3452, 3196, 3044, 2848, 1685, 1642, 1617, 1565, 1508, 1466, 1345, 1254, 1176, 1069, 918$. 1H NMR ($CDCl_3$, 250 MHz): $\delta = 10.73$ (s, 1H, NH), 9.08–9.01 (m, 3H), 8.76 (d, $J = 7.7$ Hz, 1H), 8.36–7.90 (m, 7H), 7.78 (d, $J = 8.5$ Hz, 2H), 5.78 (s, 2H, CH_2), 5.71 (s, 2H, CH_2). Anal. calcd for $C_{21}H_{17}ClN_6O_4$ (452.85): C, 55.70; H, 3.78; N, 18.56; found: C, 55.59; H, 3.77; N, 18.59.

1-(2-Oxo-2-(phenylamino)ethyl)-4-((4-oxobenzod[1,2,3]triazin-3(4H)-yl)methyl)pyridin-1-ium chloride (8i)

Yellow solid; yield: 78%; mp: 170–172 °C. IR (KBr): $\nu = 3186, 3045, 1694, 1640, 1598, 1547, 1466, 1310, 1253, 1075, 1016, 908$. 1H NMR ($CDCl_3$, 250 MHz): $\delta = 10.58$ (s, 1H, NH), 8.99 (s, 2H), 8.15 (s, 2H), 7.54–7.06 (m, 9H), 5.93 (s, 2H), 5.64 (s, 2H). ^{13}C NMR ($CDCl_3$, 62.9 MHz): $\delta = 163.5, 156.9, 146.6$ (2C), 139.5, 138.5, 136.2, 133.8, 129.4, 125.7(2C), 125.0, 124.4, 119.6 (2C), 62.0, 52.2. Anal. calcd for $C_{21}H_{18}ClN_5O_2$ (407.85): C, 61.84; H, 4.45; N, 17.17; found: C, 61.86; H, 4.41; N, 17.08.

1-(2-Oxo-2-(p-tolylamino)ethyl)-4-((4-oxobenzod[1,2,3]triazin-3(4H)-yl)methyl)pyridin-1-ium chloride (8j)

Cream solid; yield: 65%; mp: 160–162 °C. IR (KBr): $\nu = 3425, 2924, 2854, 1685, 1604, 1577, 1512, 1459, 1414, 1330, 1054, 917$. 1H NMR ($CDCl_3$, 250 MHz): $\delta = 11.22$ (s, 1H, NH), 9.03 (d, $J = 5$ Hz, 2H), 8.25–7.96 (m, 6H), 7.51 (d, $J = 7.5$ Hz, 2H), 7.10 (d, $J = 7.5$ Hz, 2H), 5.95 (s, 2H, CH_2), 5.70 (s, 2H, CH_2), 2.21 (s, 3H, CH_3). ^{13}C NMR ($CDCl_3$, 62.9 MHz): $\delta = 163.3, 156.8, 155.6, 146.6$ (2C), 144.3, 136.1, 133.7, 133.2, 129.6 (2C), 128.7(2C), 125.7 (2C), 125.0, 120.07, 119.5 (2C), 62.1, 52.2, 20.8. Anal. calcd for $C_{22}H_{20}ClN_5O_2$ (421.88): C, 62.63; H, 4.78; N, 16.60; found: C, 62.73; H, 4.68; N, 16.61.

1-(2-((4-Methoxyphenyl)amino)-2-oxoethyl)-4-((4-oxobenzod[1,2,3]triazin-3(4H)-yl)methyl)pyridin-1-ium chloride (8k)

Cream solid; yield: 52%; mp: 201–203 °C. IR (KBr): $\nu = 3423, 3030, 2855, 1686, 1604, 1578, 1510, 1471, 1428, 1293, 1059, 912$. 1H NMR ($CDCl_3$, 250 MHz): $\delta = 10.45$ (s, 1H, NH), 9.06 (d, $J = 5$ Hz, 2H), 8.25–7.95 (m, 6H), 7.40 (d, $J = 7.5$ Hz, 2H), 6.84 (d, $J = 7.5$ Hz, 2H), 5.90 (s, 2H, CH_2), 5.71 (s, 2H, CH_2). Anal. calcd for $C_{22}H_{20}ClN_5O_3$ (437.88): C, 60.34; H, 4.60; N, 15.99; found: C, 60.28; H, 4.68; N, 15.88.

1-(2-((3,4-Dimethoxyphenyl)amino)-2-oxoethyl)-4-((4-oxobenzod[1,2,3]triazin-3(4H)-yl)methyl)pyridin-1-ium chloride (8l)

Cream solid; yield: 81%; mp: 190–192 °C. IR (KBr): $\nu = 3224, 3171, 3045, 2922, 2840, 1697, 1643, 1596, 1540, 1491, 1401, 1248, 1090, 918, 829$. 1H NMR ($CDCl_3$, 250 MHz): $\delta = 10.39$ (s, 1H, NH), 9.00 (s, 2H), 8.14–7.93 (m, 6H), 7.18 (s, 1H), 6.88–6.80 (m, 2H), 5.88 (s, 2H, CH_2), 5.65 (s, 2H, CH_2). ^{13}C NMR ($CDCl_3$, 62.9 MHz): $\delta = 162.7, 156.6, 155.1, 148.5, 146.3$ (2C), 144.0, 136.4, 133.9, 131.7, 128.7, 125.7 (2C), 125.0, 124.4, 119.7, 112.4, 111.6, 104.6, 61.8, 56.6, 56.1, 52.3. Anal. calcd for $C_{23}H_{22}ClN_5O_4$ (467.9): C, 59.04; H, 4.74; N, 14.97; found: C, 59.13; H, 4.75; N, 14.87.

1-(2-((4-Chlorophenyl)amino)-2-oxoethyl)-4-((4-oxobenzod[1,2,3]triazin-3(4H)-yl)methyl)pyridin-1-ium chloride (8m)

Yellow solid; yield: 87%; mp: 140–142 °C. IR (KBr): $\nu = 3225, 3172, 3044, 2925, 2849, 1698, 1642, 1596, 1541, 1491, 1401, 1248, 1090, 918, 829$. 1H NMR ($CDCl_3$, 250 MHz): $\delta = 10.73$ (s, 1H, NH), 9.02 (d, $J = 5.5$ Hz,

2H), 8.17–7.91 (m, 6H), 7.52 (d, $J=8.25$ Hz, 2H), 7.31 (d, $J=8.25$ Hz, 2H), 5.91 (s, 2H, CH₂), 5.69 (s, 2H, CH₂). ¹³C NMR (CDCl₃, 62.9 MHz): $\delta=163.6, 156.8, 155.6, 146.5$ (2C), 144.1, 137.3, 136.3, 133.9, 129.3 (2C), 128.7, 127.9, 125.7 (2C), 125.0, 121.3, 119.9 (2C), 61.9, 52.3. Anal. calcd for C₂₁H₁₇Cl₂N₅O₂ (442.3): C, 57.03; H, 3.87; N, 15.83; found: C, 57.05; H, 3.85; N, 15.89.

1-(2-((2,3-Dichlorophenyl)amino)-2-oxoethyl)-4-((4-oxobenzod[1,2,3]triazin-3(4H)-yl)methyl)pyridin-1-ium chloride (8n)

Cream solid; yield: 89%; mp: 117–119 °C. IR (KBr): $\nu=3425, 2924, 2854, 1682, 1642, 1604, 1577, 1512, 1459, 1299, 1054, 979, 917$. ¹H NMR (CDCl₃, 250 MHz): $\delta=10.96$ (s, 1H, NH), 9.13 (d, $J=5$ Hz, 2H), 8.21–8.02 (m, 4H), 7.93 (t, $J=6.25$ Hz, 2H), 7.67 (d, $J=7.5$ Hz, 1H), 7.43 (d, $J=6.75$ Hz, 1H), 7.33 (d, $J=6.25$ Hz, 1H), 5.95 (s, 2H, CH₂), 5.87 (s, 2H, CH₂). ¹³C NMR (CDCl₃, MHz): $\delta=164.7, 156.9, 155.6, 146.7$ (2C), 144.2, 136.4, 136.1, 133.7, 132.4, 128.7, 128.4 (2C), 127.7, 125.8 (2C), 125.2, 125.0, 120.0, 62.0, 52.2. Anal. calcd for C₂₁H₁₆Cl₃N₅O₂ (476.74): C, 52.91; H, 3.38; N, 14.69; found: C, 52.98; H, 3.31; N, 14.79.

1-(2-((4-Bromophenyl)amino)-2-oxoethyl)-4-((4-oxobenzod[1,2,3]triazin-3(4H)-yl)methyl)pyridin-1-ium chloride (8o)

Cream solid; yield: 72%; mp: 140–142 °C. IR (KBr): $\nu=3438, 3171, 2925, 2852, 1694, 1604, 1545, 1488, 1464, 1331, 1271, 1007, 920$. ¹H NMR (CDCl₃, 250 MHz): $\delta=11.56$ (s, 1H, NH), 9.06 (s, 2H), 8.22–7.94 (m, 6H), 7.61 (d, $J=7.5$ Hz, 2H), 7.47 (d, $J=7.5$ Hz, 2H), 5.94 (s, 2H, CH₂), 5.74 (s, 2H, CH₂). ¹³C NMR (CDCl₃, 62.9 MHz): $\delta=163.9, 156.9, 155.6, 146.7$ (2C), 144.3, 138.2, 136.1, 133.7, 132.1 (2C), 128.7, 125.8 (2C), 125.0, 121.5, 120.1 (2C), 115.9, 62.2, 52.2. Anal. calcd for C₂₁H₁₇BrClN₅O₂ (486.75): C, 51.82; H, 3.52; N, 14.39; found: C, 51.70; H, 3.51; N, 14.38.

1-(2-((4-Nitrophenyl)amino)-2-oxoethyl)-4-((4-oxobenzod[1,2,3]triazin-3(4H)-yl)methyl)pyridin-1-ium chloride (8p)

Yellow solid; yield: 73%; mp: 178–180 °C. IR (KBr): $\nu=3453, 3197, 3044, 2849, 1684, 1643, 1617, 1565, 1507, 1466, 1344, 1258, 1179, 1071, 918$. ¹H NMR (CDCl₃, 250 MHz): $\delta=11.26$ (s, 1H, NH), 8.99 (d, $J=6.25$ Hz, 2H), 8.27–8.09 (m, 6H), 7.96 (t, $J=7.75$ Hz, 2H), 7.78 (d, $J=9$ Hz, 2H), 5.96 (s, 2H, CH₂), 5.69 (s, 2H, CH₂). ¹³C NMR (CDCl₃, 62.9 MHz): $\delta=164.8, 157.2, 155.6, 146.7$

(2C), 144.6, 144.3, 143.1, 136.1, 133.7, 128.8, 125.8 (2C), 125.6 (2C), 125.0, 120.1, 119.5 (2C), 62.2, 52.3. Anal. calcd for C₂₁H₁₇ClN₆O₄ (452.85): C, 55.70; H, 3.78; N, 18.56; found: C, 55.57; H, 3.91; N, 18.50.

Results and discussion

Chemistry

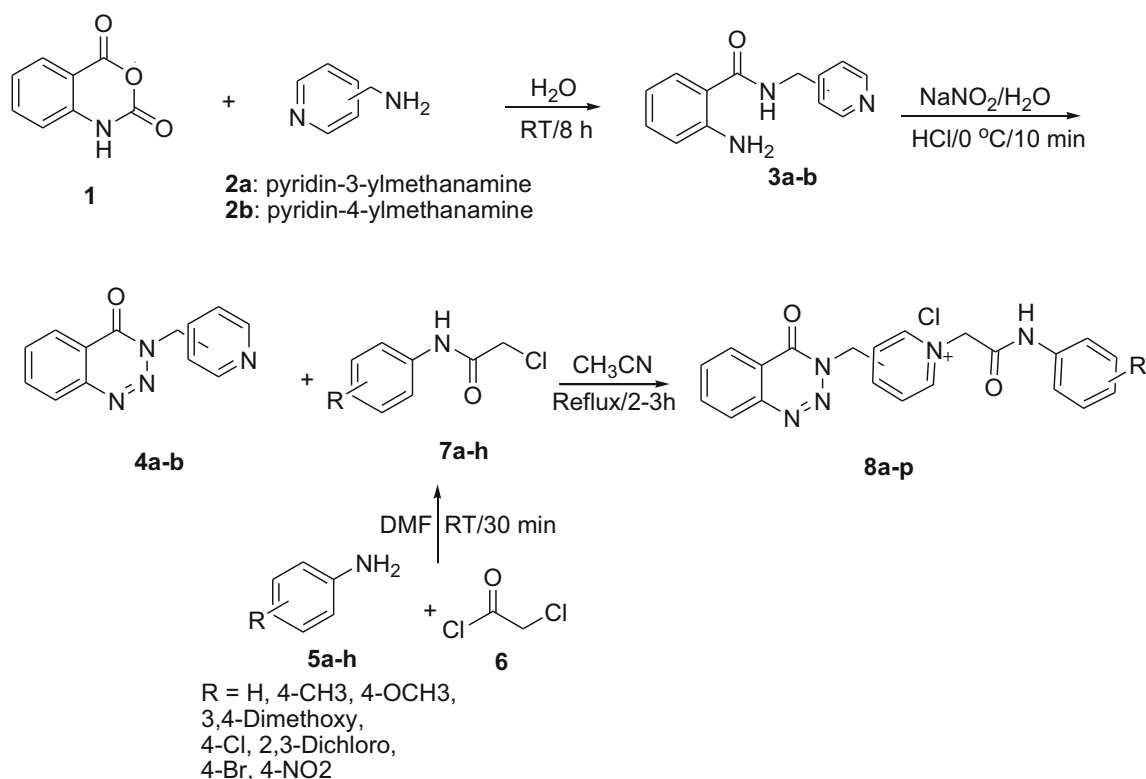
The synthetic pathway for the preparation of the 4-oxobenzod[1,2,3]-triazin-pyridinium-phenylacetamides **8a–p** is depicted in Scheme 1. It began from the reaction between isatoic anhydride **1** and pyridin-3-ylmethanamine **2a** or pyridin-4-ylmethanamine **2b** in H₂O at room temperature to give pyridine derivatives **3a–b**. Compounds **3a–b** in the presence of sodium nitrite and hydrochloride acid (in H₂O) at 0 °C were converted to 4-oxobenzod[1,2,3]-triazin-pyridine derivatives **4a–b**. On the other hand, *N*-phenyl-2-chloroacetamides **7a–h** were prepared by the reaction between aniline derivatives **5a–h** and chloroacetyl chloride **6** in DMF at room temperature. Finally, 4-oxobenzod[1,2,3]-triazin-pyridine derivatives **4a–b** reacted with *N*-phenyl-2-chloroacetamides **7a–h** in acetonitrile at reflux to give the desired compounds **8a–p**.

Cholinesterase inhibitory assay

4-Oxobenzod[1,2,3]-triazin-pyridinium-phenylacetamides **8a–p** were evaluated for their in vitro AChE/BuChE inhibitory activities. The IC₅₀ values of these compounds in comparison to standard inhibitor donepezil are listed in Table 1. The ChE inhibitory activities of the compounds **8a–p** demonstrated that all these compounds showed moderate AChE inhibitory activity (IC₅₀ = 2.0 ± 0.1–6.5 ± 0.1 μM) in comparison with the donepezil (IC₅₀ = 0.029 ± 0.006 μM) while all the synthesized compounds showed excellent BuChE inhibitory activity (IC₅₀ = 0.065 ± 0.002–0.279 ± 0.023 μM) in comparison with donepezil (IC₅₀ = 3.2 ± 0.3 μM).

Structurally, 4-oxobenzod[1,2,3]-triazin-pyridinium-phenylacetamides **8a–p** could be divided into two series: 3-pyridinium derivatives **8a–h** and 4-pyridinium derivatives **8i–p**.

The inhibitory activity of 3-pyridinium series against AChE demonstrated that 4-nitro derivative **8h** showed the most potent activity, while 4-methyl and 4-methoxy derivatives **8b** and **8c** were less active compounds. Removal of 4-nitro substituent, and or replacement of this substituent with bromine atom, led to a significant decrease in the inhibitory activity (compound **8h** vs. compounds **8a** and **8g**). Moreover, the introduction of 3,4-dimethoxy or 2,3-dichloro on pendant phenyl group did



Scheme 1 Synthesis of 4-oxobenzod[1,2,3-triazin-pyridinium-phenylacetamides **8a-p**.

not improve inhibitory activity as observed in the compounds **8d** and **8f**.

The observed IC₅₀ values of 4-pyridinium series against AChE revealed that the better results were obtained with 4-nitro, 2,3-dichloro, 4-chloro, 4-methyl substituents (compounds **8p**, **8n**, **8m**, and **8j**). In this series, 4-methoxy and 3,4-methoxy derivatives **8k** and **8l** were the less active compounds. Moreover, un-substituted compound **8i** and 4-bromo derivative **8o** also showed moderate activity against AChE.

The comparison of IC₅₀ values of 3-pyridinium derivatives **8a-h** with their corresponding 4-pyridinium analogs **8i-p** against AChE revealed that 4-pyridinium derivatives were more potent than their regioisomers.

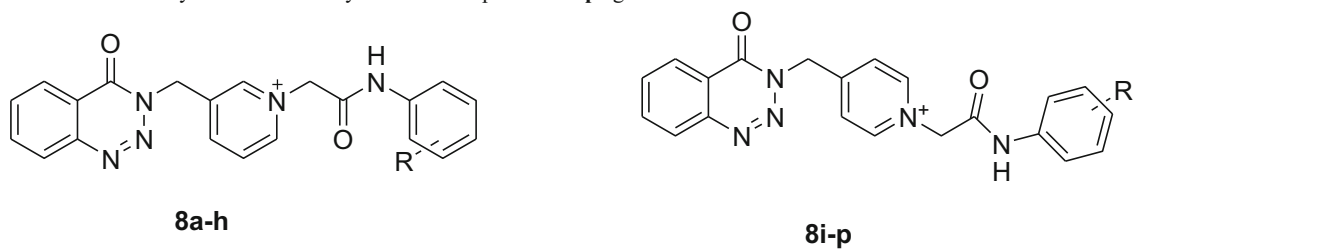
In the term of BuChE inhibitory activity in 3-pyridinium series, compounds **8e**, **8f**, and **8b** with 4-chloro, 2,3-dichloro, and 4-methyl substituents on pendant phenyl group showed highest inhibitory activities. The fourth potent compound in this series was un-substituted derivative **8a**. The introduction of 4-methoxy substituent on the pendant phenyl ring of the compound **8a**, as in compound **8c**, slightly decreased inhibitory activity. The addition of the second methoxy group onto 3-position of the pendant phenyl ring led to a significant decrease in the inhibitory activity (compound **8c** vs. **8d**). Moreover, the introduction of 4-bromo or 4-nitro on the

pendant phenyl group did not improve anti-BuChE activity as observed in compounds **8g-h**.

In the 4-pyridinium series (compounds **8i-p**), compounds **8k**, **8p**, and **8j** with 4-methoxy, 4-nitro, and methyl substituents, respectively, were the most active compounds against BuChE. The less active compound in this series was un-substituted compound **8i**. The trend of the inhibitory activity of the remaining compounds, based on the substituent on pendant phenyl ring, was 2,3-dichloro (compound **8n**) > 4-Cl (compound **8m**) > 4-Br (compound **8o**) > 3,4-dimethoxy (compound **8l**).

As can be seen in the Table 1, 3-pyridinium derivatives **8a-b** and **8d-g** were more potent than their regioisomers of 4-pyridinium series. In contrast, 4-pyridinium derivatives **8c** and **8p** were significantly more active than their corresponding 3-pyridinium regioisomers **8c** and **8h**.

The comparison of IC₅₀ values of 4-oxobenzod[1,2,3-triazin-pyridinium-phenylacetamides **8a-p** with our previous reported compounds **A** against AChE revealed that compounds **A** were more active than compounds **8a-p** (Fig. 1) [11]. In contrast, the anti-BuChE activity of the compounds **8a-p** was significantly more than compounds **A**. Moreover, AChE and BuChE inhibitory activities of the compounds **8a-p** are more than phenylacetamide derivatives **B** (Fig. 1) [12].

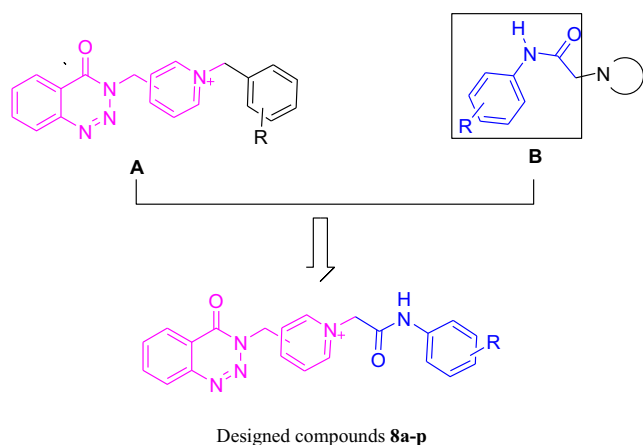
Table 1 Inhibitory activities of the synthesized compounds **8a–p** against AChE/BuChE


Compound	R	AChE IC ₅₀ (μM)	BuChE IC ₅₀ (μM)
8a	H	5.6 ± 0.2	0.097 ± 0.003
8b	4-CH ₃	6.5 ± 0.1	0.075 ± 0.004
8c	4-OCH ₃	5.9 ± 0.3	0.107 ± 0.004
8d	3,4-Dimethoxy	4.7 ± 0.2	0.193 ± 0.003
8e	4-Cl	4.7 ± 0.1	0.065 ± 0.002
8f	2,3-Dichloro	4.1 ± 0.1	0.073 ± 0.006
8g	4-Br	5.6 ± 0.5	0.147 ± 0.001
8h	4-NO ₂	2.8 ± 0.1	0.165 ± 0.003
8i	H	3.1 ± 0.1	0.279 ± 0.023
8j	4-CH ₃	2.2 ± 0.1	0.107 ± 0.001
8k	4-OCH ₃	4.7 ± 0.4	0.085 ± 0.003
8l	3,4-Dimethoxy	3.9 ± 0.1	0.223 ± 0.001
8m	4-Cl	2.0 ± 0.1	0.190 ± 0.014
8n	2,3-Dichloro	1.9 ± 0.8	0.173 ± 0.16
8o	4-Br	3.5 ± 0.1	0.203 ± 0.004
8p	4-NO ₂	1.9 ± 0.2	0.094 ± 0.001
Donepezil	–	0.029 ± 0.006	3.2 ± 0.302

Kinetic study

The kinetic study of the most potent BuChE inhibitor **8e** was performed in order to determine the inhibition mode of this compound. As can be seen in Fig. 2a, the graphical analysis of the Lineweaver–Burk reciprocal plots demonstrated that the

compound **8e** inhibited BuChE in a mixed-type inhibition mode. Therefore, this compound can interact with both the catalytic anionic site (CAS) and peripheral anionic site (PAS) of BuChE. The K_i value of the compound **8e** was calculated by using secondary re-plots of the slope versus the different concentrations of the compound **8e** and was 23.07 nM (Fig. 2b).

**Fig. 1** Design strategy for new ChE inhibitors **8a–p**

Molecular modeling studies

Reliability of induced fit docking protocol

The applied docking procedure reliability was validated by re-docking of donepezil and tacrine over AChE (6o4w) and BuChE (4bds), respectively, based on induced fit docking procedure (IFD). The docked conformations corresponding to the lowest IFD score were selected as the most possible binding modes. The RMSD was calculated for each ligand to measure the docking prediction accuracy. The pose was counted optimal if its RMSD found to be less than 2 Å. The RMSD of the re-docked

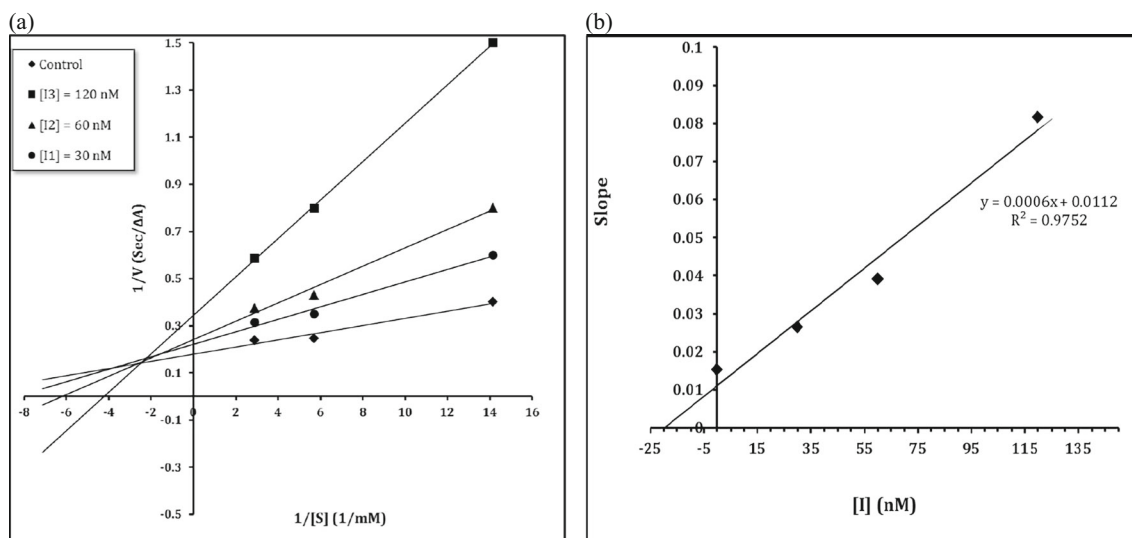


Fig. 2 **a** Lineweaver–Burk plot for the inhibition of BuChE by compound **8e** at different concentrations of ACh. **b** Steady-state inhibition constant (K_i) of compound **8e**

conformations of donepezil and tacrine over 604w and 4bds was 0.40 Å and 0.29 Å, respectively, which is considered as successfully docked [19, 20]. As a result, the validity of IFD parameters is reasonable in order to predict the related co-crystallized structures.

Docking of donepezil over AChE active site showed that the ring center of the benzyl and the inden moiety interacted with binding pocket by establishing two π - π stacking with Trp86 and Trp286, respectively. Also, the quaternary amine of piperidine ring interacts with the ring center of Trp86 and Phe338 and carbonyl unit of inden ring forms a hydrogen bond with NH unit of Phe295 in the backbone by two π -cation interactions (2.3 Å) (Fig. 3a).

Furthermore, docking of tacrine over BuChE showed the prominent role of Trp82 and His438 in stabilizing the ligand in the binding pocket by constructing π - π stacking and π -cation interactions with the aromatic part of

acridine moiety and hydrogen bond with the quaternary amine at the distance of 2.5 Å, respectively (Fig. 3b).

Investigating BuChE selectivity based on molecular dynamic simulation

In order to study the origin of BuChE selectivity of the synthesized compounds and represent their stable dynamic interaction over BuChE, it is necessary to uncover the structural perturbations incurred by the most potent BuChE inhibitor **8e**, the most potent AChE inhibitor **8p**, and the reference compound (donepezil) over ChEs and the effect of these compounds on the active site environment. The appropriate pose for MD simulation procedure of the compounds was achieved by IFD method. The stability of protein-ligand complex trajectory is defined by RMSD of the protein's C α from its initial to final conformation over 20 ns MD simulation time (Fig. 4). The

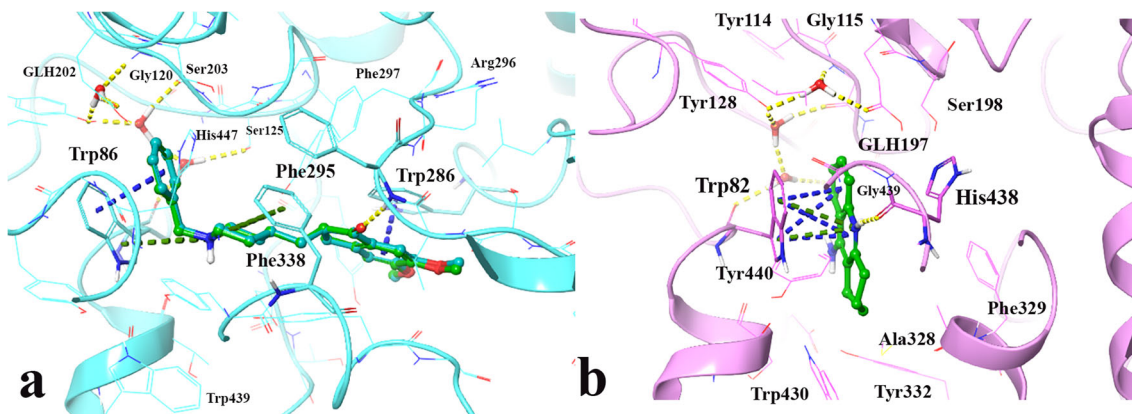


Fig. 3 Close-up representation of binding interactions of the superposed docked (green) and co-crystallized donepezil and tacrine (cyan) over AChE (**a**) and BuChE (**b**), respectively, structural waters and their hydrogen interaction render in stick

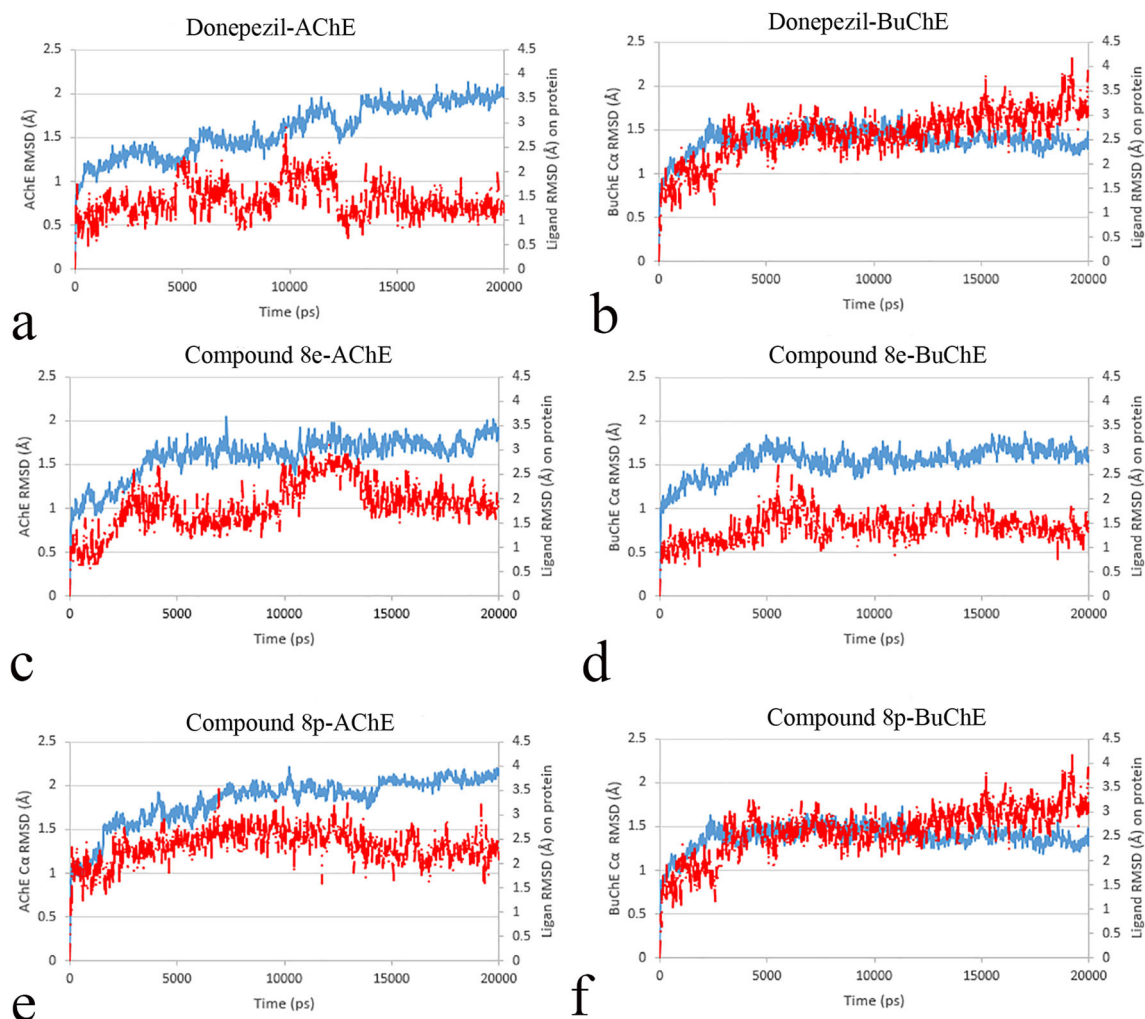


Fig. 4 RMSD of ligand (red) and protein C α (blue) for donepezil-AChE (**a**), donepezil-BuChE (**b**), **8e**-AChE (**c**), **8e**-BuChE (**d**), **8p**-AChE (**e**), and **8p**-BuChE (**f**) over 20 ns MD simulation time

RMSD of protein and ligand simulation showed that the compounds complexed with AChE maintained an overall stability throughout the last 5 ns of MD simulation time with the highest fluctuation stabilizing at an average of 2.2 Å (Fig. 4a, c, e), while the complex of the compounds with BuChE displayed longer equilibration time (about the last 15 ns) with lower fluctuations (Fig. 4b, d, f). The RMSD value of each protein-ligand complex indicates that the employed simulation time has been enough to obtain an equilibrium structure. Thus, the structures at the MD equilibrium state were used to investigate the structural specificity of the ligand-protein complexes.

For compound **8e** (Fig. 5a), the 4-oxobenzod[1,2,3]triazin-3(4H)-yl moiety was inserted deeply into the bottom of the acyl pocket (residues colored in green) of BuChE and formed strong π - π stacking interactions with the aromatic side chain of Trp231 and Phe329, which lasts for 32% and 67% of simulation time, respectively. The protonated nitrogen atom on the pyridine ring and NH unit of amide

group formed a salt bridge and water-mediated hydrogen bond with Asp74 and Thr120, respectively, during the whole time of equilibration. These can provide strong intermolecular recognitions between compound **8e** and the PAS region of BuChE, which further improved its binding affinity. The terminal phenyl group pointed to the choline-binding pocket of CAS and formed strong π - π stacking interactions for about 62% of equilibrated MD time with the aromatic side chain of Trp82 known as secondary door of ChEs active site [21]. In addition, carbonyl unit of the amide group formed a water-mediated hydrogen bond with His438 (during 66% of MD time), which belongs to the catalytic triad of CAS.

On the other way, compound **8e** became bound to AChE (Fig. 5b) in which the 4-oxobenzod[1,2,3]triazin-3(4H)-yl moiety acted as the binder for choline-binding pocket of CAS by interacting with the side chains of Trp84 through π - π interaction (T-shape) for 79% of MD time. In this way, Asp74 interacted to pyridinium ring and NH unit of amide group through a salt bridge and a hydrogen bond, respectively,

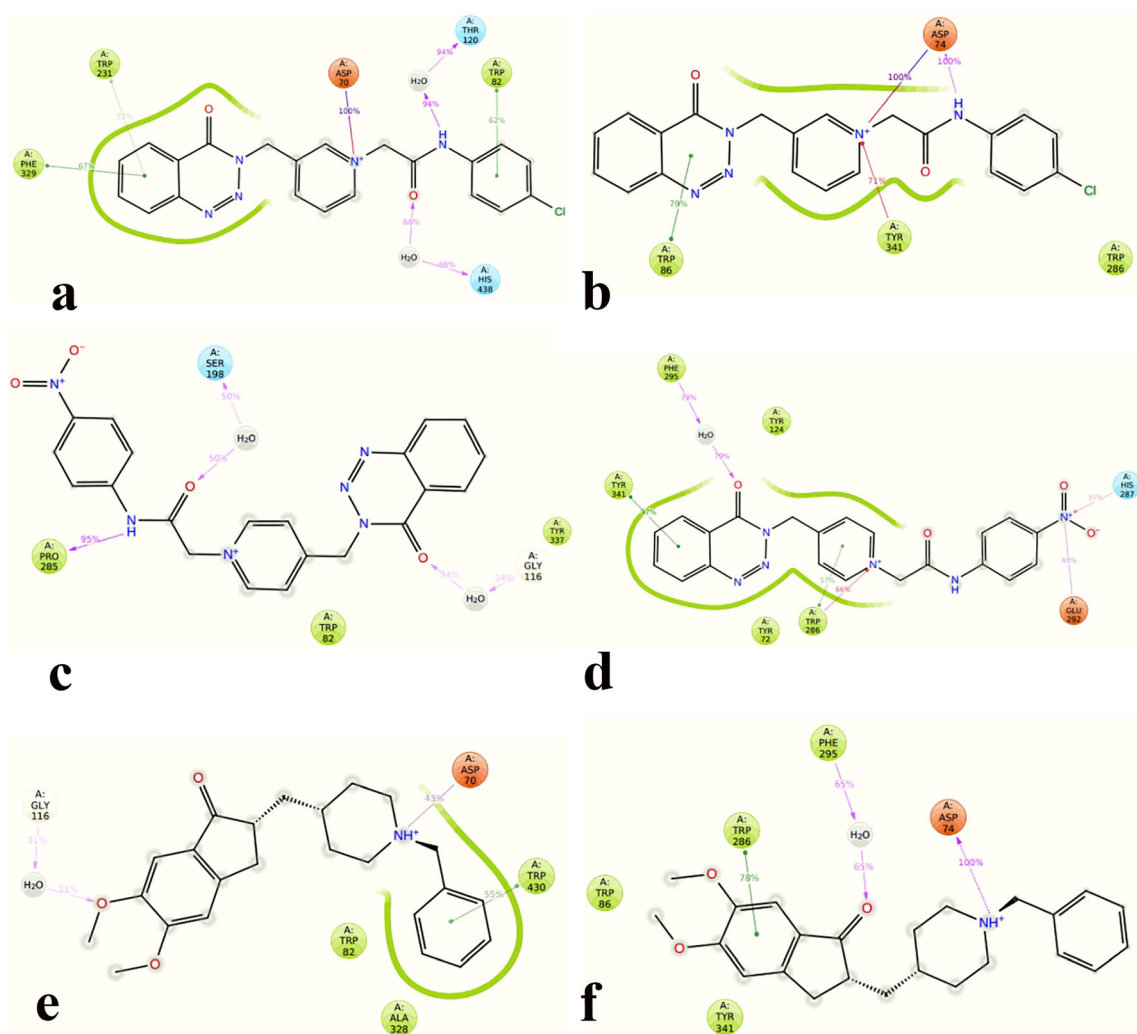


Fig. 5 2D-representation of ligand-residue interactions that occur more than 30.0% of the simulation time at the last 5 ns simulations (equilibrated simulation phase) for complex **8e**-BuChE (**a**), **8e**-AChE (**b**), **8p**-BuChE (**c**), **8p**-AChE (**d**), donepezil-BuChE (**e**), and donepezil-AChE (**f**)

for the completely equilibrated MD time. Moreover, the aromatic side chain of Tyr341 further stabilized the pyridinium ring through a π -cation interaction (during 71% of MD time).

Comparing to the interaction of AChE, compound **8e** interacted to all four parts of BuChE gorge cavity including PAS, catalytic residue, and choline- and acyl-binding pocket, while the MD simulation time highlighted PAS and choline-binding pocket as the main area which was affected by compound **8e** over AChE enzyme.

Like compound **8e**, compound **8p** positioned deeply into the BuChE active site (Fig. 5c). The ring center of pyridine ring stabilized into the choline-binding pocket of CAS by interacting with the aromatic side chains of Trp84 through hydrophobic interaction. Also, the 4-oxobenzo[d][1,2,3]triazin-3(4H)-yl moiety (4-oxo) stabilized to the Gly116 located at the oxonium hole of gorge cavity through water-mediated hydrogen bond during 31% of MD time. The amide group formed a hydrogen bond and a water-mediated hydrogen

bond with Pro285 at the acyl-binding pocket of CAS and Ser198 as the catalytic residue, respectively.

Considering Fig. 5d, compound **8p** became bound to AChE in which the 4-oxobenzo[d][1,2,3]triazin-3(4H)-yl moiety interacted to the Phe295 located at the acyl-binding pocket of CAS through water-mediated hydrogen bond during 79% of MD time. Again, like the **8e**-AChE complex, the rest of the compound **8p** located in the PAS in which the pyridinium ring formed salt bridge and π - π interaction with Trp286 for more than half of the simulation time. Furthermore, the nitro group pointed toward the outer part of PAS and formed salt bridge and water-mediated hydrogen bond with Glu292 and His287, respectively.

Comparing the interaction of compound **8p** over AChE and BuChE gorge cavity showed that it stabilized BuChE through interaction with the oxonium hole, catalytic residue, and acyl- and choline-binding pocket at the same time, while in the case of AChE, except an indirect interaction to acyl-

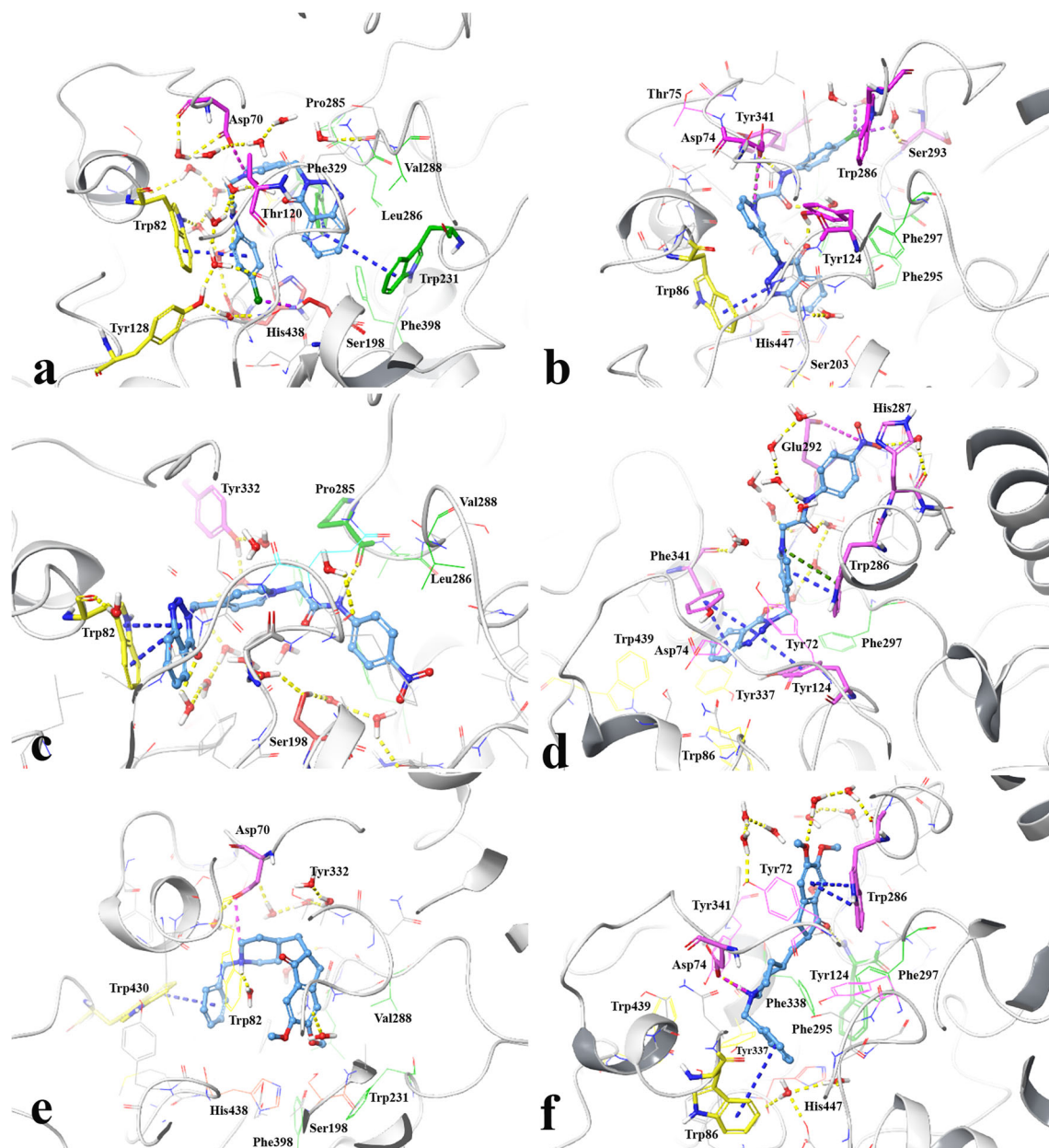


Fig. 6 Proposed binding modes for compound **8e** (a, b), **8p** (c, d), and donepezil (e, f) over BuChE and AChE, respectively. The active compound is shown as sticks and colored cyan. The acyl-binding pocket, choline-binding pocket, and catalytic residues at the CAS are in green,

yellow, and red, respectively. The PAS residues located at the top of the gorge are in purple. The hydrogen bonding, π - π stacking, and electrostatic interactions are represented as yellow, blue, and purple dashed lines, respectively

binding pocket, the main affecting region was the PAS at the top of the gorge cavity. Therefore, it can propose that interacting with the part of CAS cavity (catalytic residue, acyl- and choline-binding pocket) which is located deeper to the gorge cavity is essential for ChE selectivity. This finding can be addressed to the interaction mode of donepezil, as a selective AChE inhibitor. Considering Fig. 5e and f, donepezil stabilized to the PAS of AChE through interacting with the Asp74, Trp286, and Tyr341 during prolonged amount of MD time. In addition, it covered choline-binding pocket and acyl-

binding pocket through hydrophobic and water-mediated hydrogen bond interaction with Trp86 and Pro285, respectively. On the other hand, we can observe donepezil covered PAS, choline-binding pocket, and oxonium hole of BuChE with lower contribution MD time (during 45%, 55%, and 31%, respectively). Our molecular dynamics study suggests that the more interaction of ligand with the PAS, catalytic residues, and acyl- and choline-binding pockets at the same time has a significant contribution for selective inhibition of ChEs.

Table 2 The ligand interaction energy over ChEs based on MM-GBSA method

Compound	MM-GBSA (kcal/mol)	
	BuChE	AChE
8e	-84.83	-86.85
8p	-78.49	-91.86
Donepezil	-74.96	-104.70

The ligand-residue interactions and the fraction related to each type of interactions during the equilibrated MD simulation time were used to investigate ligand-protein complex interatomic (Fig. 5).

In silico conformational study of the most active compounds over ChEs gorge cavity

The representative structures based on hierarchical clustering method were used in uncovering the conformational difference between compounds **8e** and **8p** over the ChEs active site (Fig. 6). As it observed in Fig. 6a, c, e, compounds **8e**, **8p**, and donepezil became bound to BuChE in a U-shaped conformation in order to occupy the larger active site, while they became bound to AChE in a linear-shaped conformation (Fig. 6b, d, f).

Compared to the conformation in AChE, compound **8e** not only exhibited a more contracted pose in BuChE gorge cavity, but also showed flipped orientation in which 4-chloro phenyl moiety deeply inserted to the choline-binding pocket of BuChE while in the case of AChE, it pointed toward the most outer part of PAS which is close to the solvent accessible area (Fig. 6a, b). These flipping and changing of the orientation take place because of the bulky phenomena of chlorine group that is not tolerated by AChE gorge cavity. In view of larger

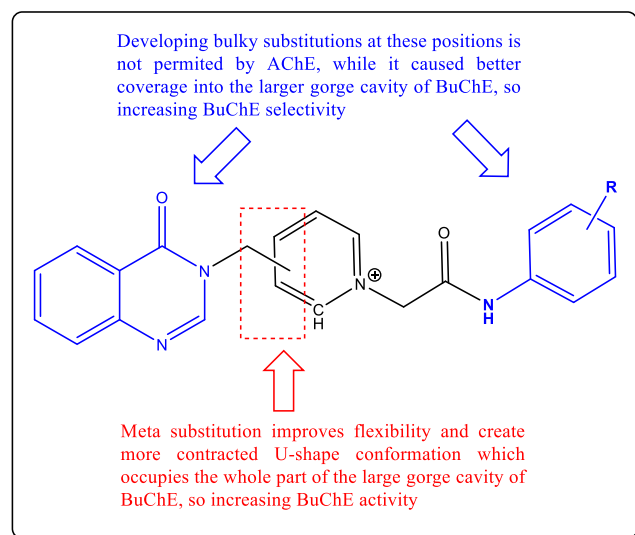


Fig. 7 Detailed modification strategy of the synthesized scaffold to improve the BuChE selectivity

gorge cavity of BuChE, developing bulky substitution at this position creates high steric clash inside the AChE narrower gorge, while it causes improved coverage into the larger gorge cavity of BuChE, so improving BuChE selectivity.

In addition to the interaction analysis, the Prime/MM-GBSA module was used to estimate the strengths of interactions between the ligand-protein complexes which were generated by the clustering method used for energy calculation (Table 2).

ΔG bind of **8e**-BuChE complex and **8p**-BhChE complex was estimated to be -84.83 and -78.49 kcal/mol, respectively, revealing stronger binding interaction of compound **8e** than **8p** which also supported by experimental assay.

Comparing Fig. 5a and c, compound **8e** generated narrower-mouth and longer length U-shape conformation than compound **8p** into the BuChE active site, which caused more coverage of PAS site and CAS through its bottom and wall of the U-shape conformation.

The reason for difference in compactness of compound **8e** and **8p** might be pointed to the difference in the position of benzo[1,2,3]triazin-3(4H) aromatic ring substitution over the pyridine ring which could affect the flexibility of the whole structure. The mentioned group existed at meta-position in compound **8e** while in case of compound **8p** it is located at para-position with less ability for bending the whole molecule. The hypothesis is consistent to some extent with our experimental enzymatic assay, in which the potent inhibition of BuChE are acquired through compounds which are related to the 3-benzo [1,2,3]triazin-3(4H) substitution over the pyridine ring rather than 4-substituted one (compounds **8e**, **8f**, **8b**, **8a**, **8c**). Therefore, besides the impact of substitutions on ChE selectivity, the core structural flexibility of compounds has outstanding role in the ChE inhibition potency. Finally, Fig. 7 summarized the two-design strategy for developing more selective and potent compound for the designed scaffold.

Conclusion

In conclusion, 16 new 4-oxobenzo[d]1,2,3-triazin-pyridinium-phenylacetamide hybrids **8a-p** were synthesized and evaluated as potent cholinesterase inhibitors for treatment of AD. The in vitro inhibition assay of these compounds revealed that all the synthesized compounds had significant inhibitory activity against BuChE. Among them, compound **8e** displayed the highest anti-BChE activity. Furthermore, kinetic study revealed that this compound inhibited BChE via a mixed-type inhibition mode. Furthermore, compound **8e** as the most potent inhibitors against BuChE was inserted well into the gorge cavity of BuChE by simultaneously interacting with CAS and PAS.

Compliance with ethical standards

Conflict of interest The authors declare that they have no conflict of interest.

References

- Burns A, Jacoby R, Levy R (1991) Neurological signs in Alzheimer's disease. *Age Ageing* 20:45–51
- Reitz C, Mayeux R (2014) Alzheimer disease: epidemiology, diagnostic criteria, risk factors and biomarkers. *Biochem Pharmacol* 88:640–651
- Masters CL, Cappai R, Barnham KJ, Villemagne VL (2006) Molecular mechanisms for Alzheimer's disease: implications for neuroimaging and therapeutics. *J Neurochem* 97:1700–1725
- Francis PT, Palmer AM, Snape M, Wilcock GK (1999) The cholinergic hypothesis of Alzheimer's disease: a review of progress. *J Neurol Neurosurg Psychiatry* 66:137–147
- Darvesh S, Hopkins DA, Geula C (2003) Neurobiology of butyrylcholinesterase. *Nat Rev Neurosci* 4:131
- Nordberg A, Ballard C, Bullock R, Darreh-Shori T, Somogyi M (2013) A review of butyrylcholinesterase as a therapeutic target in the treatment of Alzheimer's disease. *Prim Care Companion CNS Disord* 15
- Greig NH, Utsuki T, Yu QS, Zhu X, Holloway HW, Pery T, Lee B, Ingram DK, Lahiri DK (2001) A new therapeutic target in Alzheimer's disease treatment: attention to butyrylcholinesterase. *Curr Med Res Opin* 17:159–165
- Lane RM, Potkin SG, Enz A (2006) Targeting acetylcholinesterase and butyrylcholinesterase in dementia. *Int J Neuropsychopharmacol* 9:101–124
- Najafi Z, Mahdavi M, Saeedi M, Karimpour-Razkenari E, Asatouri R, Vafadamejad F, Moghadam FH, Khanavi M, Sharifzadeh M, Akbarzadeh T (2017) Novel tacrine-1, 2, 3-triazole hybrids: in vitro, in vivo biological evaluation and docking study of cholinesterase inhibitors. *Eur J Med Chem* 125:1200–1212
- Ghafary S, Najafi Z, Mohammadi-Khanaposhtani M, Nadri H, Edraki N, Ayashi N, Larjani B, Amini M, Mahdavi M (2018) Novel cinnamic acid-tryptamine hybrids as potent butyrylcholinesterase inhibitors: synthesis, biological evaluation, and docking study. *Arch Pharm* 351:1800115
- Hosseini F, Ramazani A, Mohammadi-Khanaposhtani M, Tehrani MB, Nadri H, Larjani B, Mahdavi M (2019) Design, synthesis, and biological evaluation of novel 4-oxobenzo [d] 1, 2, 3-triazin-benzylpyridinium derivatives as potent anti-Alzheimer agents. *Bioorg Med Chem* 27:2914–2922
- Tarikoğulları A, Çizmecioglu M, Saylam M, Parlar S, Alptüzün V, Soyer Z (2016) Synthesis and cholinesterase inhibitory activity of some phenylacetamide derivatives bearing 1H-pyrazole and 1H-1, 2, 4-triazole. *Marmara Pharm J* 20:21–27
- Ellman GL, Courtney KD, Andres Jr V, Featherstone RM (1961) A new and rapid colorimetric determination of acetylcholinesterase activity. *Biochem Pharmacol* 7:88–95
- Schrodinger LLC (2009) Schrodinger suite 2012 induced fit docking protocol; glide version 5.8. New York
- Gerlits O, Ho KY, Cheng X, Blumenthal D, Taylor P, Kovalevsky A, Radic ZA (2019) New crystal form of human acetylcholinesterase for exploratory room-temperature crystallography studies. *Chem Biol Interact* 309:108698–108698
- Nachon F, Carletti E, Ronco C, Trovaslet M, Nicolet Y, Jean L, Renard P (2013) Crystal structures of human cholinesterases in complex with Huprine W and tacrine: elements of specificity for anti-Alzheimer's drugs targeting acetyl- and butyrylcholinesterase. *Biochem J* 453:393–399
- Rosenberry T, Brazzolotto X, Macdonald I, Wandhammer M, Trovaslet-Leroy M, Darvesh S, Nachon F (2017) Comparison of the binding of reversible inhibitors to human butyrylcholinesterase and acetylcholinesterase: a crystallographic, kinetic and calorimetric study. *Molecules* 22:2098
- Asadi M, Ebrahimi M, Mohammadi-Khanaposhtani M, Azizian H, Sepehri S, Nadri H, Biglar M, Amanlou M, Larjani B, Mirzazadeh R, Mahdavi M (2019) Design, synthesis, molecular docking, and cholinesterase inhibitory potential of phthalimide-dithiocarbamate hybrids as new agents for treatment of Alzheimer's disease. *Chem Biodivers*. <https://doi.org/10.1002/cbdv.201900370>
- Erickson JA, Jalaie M, Robertson DH, Lewis RA, Vieth M (2004) Lessons in molecular recognition: the effects of ligand and protein flexibility on molecular docking accuracy. *J Med Chem* 47:45–55
- Nissink JWM, Murray C, Hartshorn M, Verdonk ML, Cole JC, Taylor R (2002) A new test set for validating predictions of protein–ligand interaction. *Proteins Struct Funct Genet* 49:457–471
- Vyas S, Beck JM, Xia S, Zhang J, Hadad CM (2010) Butyrylcholinesterase and G116H, G116S, G117H, G117N, E197Q and G117H/E197Q mutants: a molecular dynamics study. *Chem Biol Interact* 187:241–245

Publisher's note Springer Nature remains neutral with regard to jurisdictional claims in published maps and institutional affiliations.